

Trapped-atom cooling beyond the Lamb-Dicke limit using electromagnetically induced transparency

Maryam Roghani* and Hanspeter Helm†

Institute of Physics, Albert Ludwigs University, Hermann-Herderstrasse 3, D-79104 Freiburg, Germany

(Received 8 March 2008; published 24 April 2008)

We investigate the cooling of trapped atoms by electromagnetically induced transparency under conditions of weak confinement and beyond the Lamb-Dicke limit, i.e., the spontaneous decay width is large compared to the trap oscillation frequency and the recoil energy is a substantial fraction of the vibrational energy spacing of the trap. Numerical solutions of the Liouville equation for a density matrix describing states of vibrational and electronic degrees of freedom show that vibrational cooling is feasible at even substantial values of the Lamb-Dicke parameter and under conditions of weak confinement, a situation where sideband pumping is inefficient. Our approach permits us to predict cooling efficiency and cooling rates under realistic experimental conditions for neutral atoms in optical dipole traps.

DOI: [10.1103/PhysRevA.77.043418](https://doi.org/10.1103/PhysRevA.77.043418)

PACS number(s): 37.10.De, 42.50.Gy, 42.50.Tx

I. INTRODUCTION

A frequent goal in atomic physics is to laser-cool trapped atoms to the lowest energy state of the trap potential. One way to cool atoms to the ground state of a trap is via two-photon processes, which might eventually even result in Bose-Einstein condensation [1,2] in an all optical way [3]. Important in this context is the Lamb-Dicke parameter [4]

$$\eta^2 = \frac{E_r}{\hbar\omega}, \quad (1)$$

which describes the ratio of the recoil energy, E_r , that the atomic center-of-mass gains in atom-photon interaction and the vibrational energy spacing, ω , of the external trap. An equivalent expression for the Lamb-Dicke parameter is in terms of the product of the ground-state trap size and the laser wave number, $\eta = a_0 k$. Also the confinement parameter, Γ/ω , with Γ being the spontaneous emission rate of the excited state is crucial in controlling vibrationally selective optical pumping.

An efficient cooling mechanism in the limit of small values of the Lamb-Dicke parameter is sideband cooling [5]. Beyond the Lamb-Dicke limit ($\eta \rightarrow 0$), two techniques, originally designed to achieve subrecoil temperatures of free atoms [6], have been proven to be effective, dark-state cooling [7], which operates with angular momentum internal transitions, and Raman cooling [8], a sequence of laser pulses followed by a repumping process.

Standard sideband cooling for trapped two-level atoms for $\eta \rightarrow 0$ consists of two stages: First, tuning one laser to the lower motional sideband of an internal transition, $\Delta = -\omega$. The detuning Δ is defined here as $\Delta = \omega_L - \omega_0$, where ω_L is the laser frequency and ω_0 is the unperturbed transition frequency of the two-level atom. This laser preferentially pumps population from an internal ground-state level $|n+1\rangle$ to the electronically excited state in trap level $|n\rangle$. The sec-

ond stage is accomplished by spontaneous emission, which transfers the population again to the atomic ground state with the relaxation rate Γ . In the Lamb-Dicke limit spontaneous emission occurs without changing the trap vibrational level. Hence, by repeatedly following this process the population would eventually assemble in the level $|g, 0\rangle$, which is a dark state in the sense that the laser is tuned to the lower motional sideband. This condition can only be satisfied in the strong confinement limit when $\Gamma \ll \omega$ [9]. In weak confinement sideband excitation is rather unselective and spontaneous emission leads to a diffusion of vibrational population over neighboring $|n\rangle$ states.

A key to overcome this problem is to use a second laser in a multilevel pumping scheme. In this way an effective two-level transition with an effective decay rate Γ_{eff} appears, which is proportional to the pump beam strength [10,11]. Therefore, by suitable choice of laser parameters the condition $\Gamma_{\text{eff}} < \omega$ can be met [12,13]. In the limit of large detuning ($\Delta \approx \Gamma > \omega$), the two-photon detuning (connecting the two ground-state levels) can be made very small, such that vibrationally diagonal optical transitions (carrier transitions) are suppressed by electromagnetically induced transparency (EIT). In this situation vibrationally off-diagonal two-photon transitions experience different transition probabilities for vibrational cooling and heating, their relative magnitude being dictated by the asymmetric absorption line profile around the dark-state resonance. The cooling rate dominates over heating when the pump laser is blue-detuned ($\Delta > 0$) and it can be optimized by choosing the separation between EIT minimum and the ac-Stark-shifted excited state level to be equal to the trap frequency. In order to define the meaning of detuning we give the state energies as $E_j = \hbar\omega_j$ with $j=1,2,3$ for a three-level Λ system, where $\omega_{31} = \omega_3 - \omega_1$ and the detuning is $\Delta = \omega_{L1} - \omega_{31}$ such as shown in Fig. 1. The asymmetry in sideband transitions for cooling and heating was analyzed by Morigi *et al.* [14,15] in the limit of small Lamb-Dicke parameter. In this limit only the first sideband transition $|n\rangle \rightarrow |n \pm 1\rangle$ is of significant strength. This method is readily realized in ion traps and indeed experiments conducted in Innsbruck [7] show that this cooling scheme can very rapidly take an ion into the ground vibrational level of a trap.

*maryam.roghani@physik.uni-freiburg.de

†helm@uni-freiburg.de

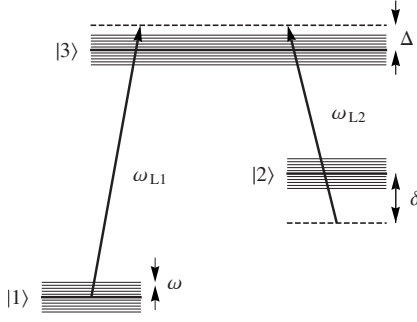


FIG. 1. Electronic configuration of the three-level atom. The thin lines signify trap vibrational levels. For the definition of the sign of the detunings Δ and δ see Eq. (7).

In this paper, we discuss the situation when the Lamb-Dicke parameter is not very small, a situation frequently encountered in optical dipole traps for neutral atoms. Here, η values are typically in the range $\eta > 0.1$, in which case effects from higher sidebands need to be considered as well. Equally important, the substantial strength of vibrationally off-diagonal vibrational transitions for even small values of η requires to explicitly account for off-diagonal transitions for proper prediction of the absorption and dispersion relation of the atom. We do this by numerically solving the Liouville equation for a density matrix describing electronic and vibrational levels.

The paper is organized as follows. We first discuss the density operator relations for the case of entanglement between electronic and vibrational states. We then present solutions for the time-dependent development of the density matrix as well as its stationary state for various values of η , including a comparison with the results predicted by the Morigi *et al.* model [14] (in the following referred to as the Lamb-Dicke limit). Finally we discuss the theoretical and experimental limitations which arise when applying the EIT scheme to cooling of neutral atoms in a far-red-detuned optical dipole trap.

II. THEORY

We consider a three-level, Λ -shaped atom trapped in a one-dimensional harmonic oscillator (HO). We explore the time-dependent evolution of the density matrix for this system by solving the Liouville equation

$$\frac{\partial \hat{\rho}}{\partial t} = -\frac{i}{\hbar} [\hat{\mathcal{H}}, \hat{\rho}] + \hat{\mathcal{L}}_0. \quad (2)$$

The density operator $\hat{\rho}$ comprises contributions from both electronic and vibrational degrees of freedom

$$\hat{\rho} = \hat{\rho}_{\text{el}} \otimes \hat{\rho}_{\text{c.m.}} = \hat{\rho} \otimes \hat{\sigma}. \quad (3)$$

The Hamiltonian $\hat{\mathcal{H}}$ describes the motion of the atomic center-of-mass (c.m.), the internal electronic configuration, and the interaction of the atom with two laser beams

$$\hat{\mathcal{H}} = \hat{\mathcal{H}}_{\text{c.m.}} + \hat{\mathcal{H}}_{\text{el}} + \hat{\mathcal{H}}_{\text{int.}} \quad (4)$$

Here

$$\hat{\mathcal{H}}_{\text{c.m.}} = p\hbar\omega|p\rangle\langle p|, \quad (5)$$

describes the quantum mechanical HO with trap frequency ω and the Fock states $|p\rangle$. The electronic configuration Hamiltonian is [16]

$$\hat{\mathcal{H}}_{\text{el}} = +\hbar\Delta|1\rangle\langle 1| + \hbar(\delta + \Delta)|2\rangle\langle 2|, \quad (6)$$

where Δ is the one-photon detuning between the electronic levels $|1\rangle$ and $|3\rangle$ and δ is the two-photon detuning between levels $|1\rangle$ and $|2\rangle$, as shown in Fig. 1,

$$\Delta = \omega_{L1} - \omega_{31},$$

$$\Delta + \delta = \omega_{L2} - \omega_{32}. \quad (7)$$

The energy differences between the respective unperturbed electronic states are $\omega_{31} = \omega_3 - \omega_1$ and $\omega_{32} = \omega_3 - \omega_2$. The interaction Hamiltonian for the two running wave laser beams is derived from the interaction picture in the rotating-wave approximation [17]

$$\begin{aligned} \hat{\mathcal{H}}_{\text{int}} = \frac{\hbar}{2} \{ & g_1^* e^{-ik_1 \cdot \vec{x}} |1\rangle\langle 3| + g_2^* e^{-ik_2 \cdot \vec{x}} |2\rangle\langle 3| + g_1 e^{ik_1 \cdot \vec{x}} |3\rangle\langle 1| \\ & + g_2 e^{ik_2 \cdot \vec{x}} |3\rangle\langle 2| \}. \end{aligned} \quad (8)$$

For solving the Liouville equation, we need the eigenbras and kets for the atomic sample. We define them as $|i, n\rangle = |i\rangle \otimes |n\rangle$, where $|i\rangle$ is the representation of the electronic levels $i=1, 2, 3$, and $|n\rangle$ is the Fock state for the atomic center-of-mass motion. Rewriting Eq. (2) for the trapped three-level atom we obtain

$$\begin{aligned} \langle i| \langle n| \frac{\partial \hat{\rho}}{\partial t} |j\rangle |m\rangle = & -\frac{i}{\hbar} \langle i| \langle n| \hat{\rho} \otimes [\hat{\mathcal{H}}_{\text{c.m.}}, \hat{\sigma}] |j\rangle |m\rangle \\ & -\frac{i}{\hbar} \langle i| \langle n| [\hat{\mathcal{H}}_{\text{el}}, \hat{\rho}] \otimes \hat{\sigma} |j\rangle |m\rangle \\ & -\frac{i}{\hbar} \langle i| \langle n| [\hat{\mathcal{H}}_{\text{int}}, \hat{\rho} \otimes \hat{\sigma}] |j\rangle |m\rangle + \langle i| \langle n| \hat{R} |j\rangle |m\rangle, \end{aligned} \quad (9)$$

where the term $\langle i| \langle n| \hat{R} |j\rangle |m\rangle$ signifies relaxation terms. In a more compact form we may write

$$\begin{aligned} \langle i, n| \frac{\partial \hat{\rho}}{\partial t} |j, m\rangle = & -\frac{i}{\hbar} \hat{\rho}_{ij} \otimes \langle n| [\hat{\mathcal{H}}_{\text{c.m.}}, \hat{\sigma}] |m\rangle \\ & -\frac{i}{\hbar} \langle i| [\hat{\mathcal{H}}_{\text{el}}, \hat{\rho}] |j\rangle \otimes \hat{\sigma}_{nm} \\ & -\frac{i}{\hbar} \langle i| [\hat{\mathcal{H}}_{\text{int}}, \hat{\rho}] |j\rangle \otimes \langle n| [\hat{\mathcal{H}}_{\text{int}}, \hat{\sigma}] |m\rangle \\ & + \langle i| \langle n| \hat{R} |j\rangle |m\rangle. \end{aligned} \quad (10)$$

After substituting (5)–(8) into (10), applying the identity operator $1 = \sum_{p=0}^{\infty} |p\rangle\langle p|$, and after some rearrangement we can rewrite Eq. (10) as

$$\begin{aligned}
\langle i, n | \frac{\partial \hat{\rho}}{\partial t} | j, m \rangle = & -i\omega\rho_{ij}(p\sigma_{pm}\delta_{p,n} - p\sigma_{np}\delta_{p,m}) \\
& -i(\Delta\delta_{i,1}\rho_{1j} + (\delta + \Delta)\delta_{i,2}\rho_{2j})\sigma_{nm} \\
& + i[\Delta\delta_{1,j}\rho_{i1} + (\delta + \Delta)\delta_{2,j}\rho_{i2}]\sigma_{nm} \\
& - \frac{i}{2} \sum_{p=1}^{\infty} [(g_1^*\rho_{3j}\delta_{i,1} + g_2\rho_{2j}\delta_{i,3}) \\
& \times \langle n | e^{-i(\vec{k}_1 - \vec{k}_2) \cdot \vec{x}} | p \rangle \sigma_{pm} \\
& + (g_1\rho_{1j}\delta_{i,3} + g_2^*\rho_{3j}\delta_{i,2}) \langle n | e^{i(\vec{k}_1 - \vec{k}_2) \cdot \vec{x}} | p \rangle \sigma_{pm} \\
& + (-g_1^*\rho_{i1}\delta_{3,j} - g_2\rho_{i3}\delta_{2,j}) \langle p | e^{-i(\vec{k}_1 - \vec{k}_2) \cdot \vec{x}} | m \rangle \sigma_{np} \\
& + (-g_2^*\rho_{i2}\delta_{3,j} - g_1\rho_{i3}\delta_{1,j}) \langle p | e^{i(\vec{k}_1 - \vec{k}_2) \cdot \vec{x}} | m \rangle \sigma_{np} \\
& + R_{in,jm}. \tag{11}
\end{aligned}$$

For the Franck-Condon factors [18] we define the abbreviation

$$\langle n | e^{\pm i\vec{k}_q \cdot \vec{x}} | p \rangle = F(n, p, \pm \eta_q), \tag{12}$$

where $q=1, 2$ refers to laser 1 and 2, respectively. The parameter η is

$$\eta_q = \sqrt{\frac{\hbar k_{\text{eff}}^2}{2M\omega}}, \tag{13}$$

where $k_{\text{eff}} = |\vec{k}_q| \cos \theta$, with θ being the angle between the HO axis and the wave vector of the respective laser beam and M being the mass of the trapped atom.

Equation (11) contains terms with $\langle p | e^{\pm i(\vec{k}_1 - \vec{k}_2) \cdot \vec{x}} | n \rangle$, which describe three-level atom interaction with an effective laser wave vector $\delta\vec{k} = \vec{k}_1 - \vec{k}_2$. For a Λ system with near-degenerate ground states (e.g., hyperfine- or Zeemann-split ground states) $\delta\vec{k}$ tends to zero for copropagating laser beams, thus effectively suppressing any motional changes in atom-laser interaction [19]. The choice of angle between the laser beams is thus crucially important for the cooling process, in controlling the magnitude of δk as well as the projection of $\delta\vec{k}$ on the trap confinement axis. The latter dictates the effective magnitude of η in two-photon transitions, thus giving the experimenter some degree of freedom in optimization.

The factor F in Eq. (12) actually describes the atomic center-of-mass transition matrix element between trap levels, as an effect of atom-light interaction. In the Lamb-Dicke limit the momentum shift operator in Eq. (12) is approximated in lowest order

$$e^{\pm i\eta(\hat{a} + \hat{a}^\dagger)} \approx 1 \pm i\eta(\hat{a} + \hat{a}^\dagger) \tag{14}$$

thus allowing only the carrier transition and the first red and blue sidebands, the latter having an absorption strength $(n+1)\eta^2$ times that of the carrier transition in the Lamb-Dicke limit.

A. Relaxation terms due to spontaneous emission

Relaxation due to spontaneous emission leads to a loss of population in the electronically excited vibrational states

$|3, n\rangle$ and gain of population by the ground-state levels $|1, n'\rangle$ and $|2, n'\rangle$, where we allow for migration of population in the vibrational manifold of the HO by spontaneous emission. Spontaneous emission also leads to a loss of coherence between different electronic and HO levels. In operator language, effects of spontaneous emission can be written by a Liouvillian operator [20]

$$\begin{aligned}
\hat{\mathcal{L}}_0 = & -\frac{\Gamma}{2} [|3\rangle\langle 3| \hat{\rho} + \hat{\rho} |3\rangle\langle 3|] + \sum_{j=1}^2 \Gamma_j \int_{-1}^{+1} d \cos \phi \Xi(\cos \phi) |j\rangle \\
& \times \langle 3 | (e^{iq_j x \cos \phi} \hat{\rho} e^{-iq_j x \cos \phi}) |3\rangle \langle j|. \tag{15}
\end{aligned}$$

The key element in controlling laser cooling and heating is the redistribution of population among the HO levels in optical pumping as well as in spontaneous emission. The latter is governed by the term $(e^{iq_j x \cos \phi} \hat{\rho} e^{-iq_j x \cos \phi})$ and the integration over the angular distribution of emitted photons, $\Xi(\cos \phi)$. We simplify this term by assuming that the spontaneously emitted photons appear along the trap axis, as discussed in Appendix A. This assumption maximizes the effect of diffusion between trap levels due to spontaneous emission.

Population gain in level $|j\rangle$ ($j=1, 2$) results from the branching of spontaneous emission into the two ground states which occurs with the rates $\Gamma_1 + \Gamma_2 = \Gamma$,

$$\mathcal{L}_{0,j,nj,n} = \Gamma_j \sum_{p=1}^{\infty} |F(n, p, \eta_S)|^2 \sigma_{pp}. \tag{16}$$

Here we have introduced η_S , the effective Lamb-Dicke parameter for spontaneous emission into level j ,

$$\eta_S = q_j \sqrt{\frac{\hbar}{2M\omega}}, \tag{17}$$

with $q_j = (\omega_3 - \omega_j)/c$. Equation (16) describes the population gain in level $|j, n\rangle$,

$$R_{jn,jn} = +\Gamma_j \rho_{33} \sum_{p=1}^{\infty} |F(n, p, \eta_S)|^2 \sigma_{pp}. \tag{18}$$

Due to population conservation we also have

$$R_{3n,3n} = -\Gamma \rho_{33} \sum_{p=1}^{\infty} |F(n, p, \eta_S)|^2 \sigma_{pp}. \tag{19}$$

The second term on the right-hand side of Eq. (15) also gives rise to coherence loss due to spontaneous emission when $n \neq m$ and contains only the coherent terms of different vibrational levels

$$\Gamma_j \rho_{33} \langle n | e^{iq_j x} \hat{\sigma} e^{-iq_j x} | m \rangle, \tag{20}$$

where again we have assumed that spontaneous emission occurs only along the trap axis,

$$R_{jn,3m} = \Gamma_j \rho_{33} \sum_{p=1}^{\infty} \sum_{o=1}^{\infty} F(n, p, \eta_S) F(o, m, -\eta_S) \sigma_{po}. \tag{21}$$

Next we consider the first term on the right-hand side of Eq. (15). It describes loss of coherence between different trap levels, due to spontaneous emission

$$R_{3n,3m} = -\Gamma \rho_{33} \sigma_{nm} (1 - \delta_{n,m}), \quad (22)$$

where the δ function has been added in order to avoid counting loss of population two times. The first term on the right-hand side of Eq. (15) also describes coherence loss between ground and excited electronic states and trap vibrational levels,

$$R_{1n,3m} = -\frac{\Gamma}{2} \rho_{13} \sigma_{nm}, \quad (23)$$

$$R_{2n,3m} = -\frac{\Gamma}{2} \rho_{23} \sigma_{nm}, \quad (24)$$

$$R_{3n,1m} = -\frac{\Gamma}{2} \rho_{31} \sigma_{nm}, \quad (25)$$

$$R_{3n,2m} = -\frac{\Gamma}{2} \rho_{32} \sigma_{nm}. \quad (26)$$

B. Numerical approach

We solve Eq. (11) numerically for a fixed number of vibrational trap levels to obtain the time dependence of cooling as well as stationary-state solutions. In the following we discuss the case of three electronic levels as shown in Fig. 1 and a number of m_m vibrational levels in each electronic state. The number of coupled equations then is $(3m_m)^2$. Typically we took m_m in the range from 10–25 vibrational levels. For simplicity we have assumed the vibrational trap spacing ω to be identical in all three electronic states, a situation not typically met in neutral atom experiments. For convenience we have also set $\eta_S = \eta_q$. Neither of these assumptions nor the restriction to a finite number of vibrational levels influences our general conclusions on EIT cooling beyond the Lamb-Dicke limit.

Convergence tests on the dependence of the stationary solutions on the number of vibrational levels included in the calculation showed that the results converge when the number of vibrational levels accounted for (m_m) is larger than the width over which substantial sidebands occur. The magnitude required for m_m can be estimated by inspecting a map of the strength of sideband transitions [21]. Examples are shown in Fig. 2. Here we give the magnitude of the squared Franck-Condon factors $|F(n, m, \eta)|^2$ from Eq. (12) for the lowest 30 vibrational levels (upper panel) and the sideband spectrum for $n=20$ (lower panel) at two values of η . Note that the Franck-Condon factors $F(n, m, \eta)$ are dimensionless and fulfill the condition $\sum_{m=0}^{m=\infty} |F(n, m, \eta)|^2 = 1$.

III. RESULTS AND DISCUSSION

The aim of our study is to examine the range of validity of EIT cooling under conditions when neither the Lamb-Dicke

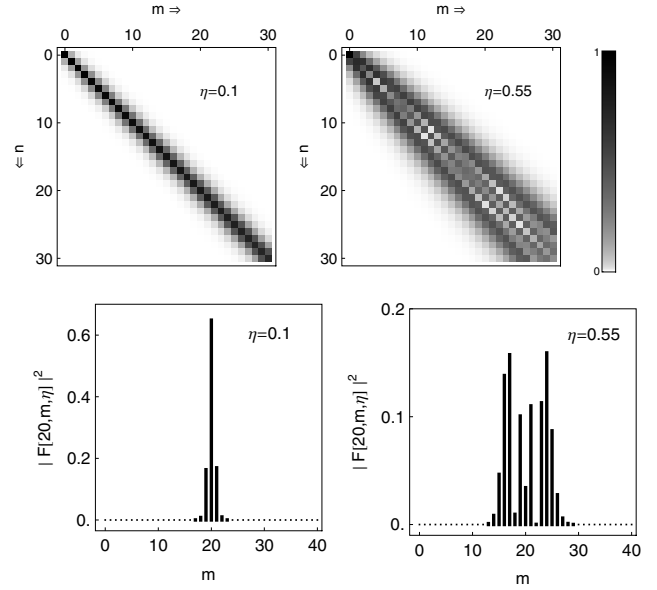


FIG. 2. Absolute values of the Franck-Condon factors $|F(n, m, \eta)|$ from Eq. (12) are shown in the upper row for two values of η . The relative strength of sideband transitions originating from $n=20$ is given in the lower row.

parameter η nor the confinement parameter Γ/ω are small. To this end we examine two limiting parameter ranges, one considered by Morigi *et al.* [14] in connection with ion traps. This allows us to make a direct comparison with the predictions for the Lamb-Dicke limit, and a second case which is realistic for neutral Rb atoms in an optical dipole trap.

We begin by considering the effect of detuning Δ on the imbalance of sideband transitions for cooling and heating in Fig. 3. Here, the purely electronic two-photon detuning δ is chosen as $\delta=0$. In this case the carrier transitions (they are diagonal in vibrational quantum number) are suppressed by the EIT minimum. The light field of the two laser beams is however experienced in a different fashion by off-diagonal (sideband) transitions. For sideband transitions involving a change in vibrational quantum number by $\Delta n = -\delta_{\text{eff}}/\omega$, the EIT condition is not satisfied. In the case that $\Delta \gg \omega$ the absorption line shape in sideband transitions is given by the

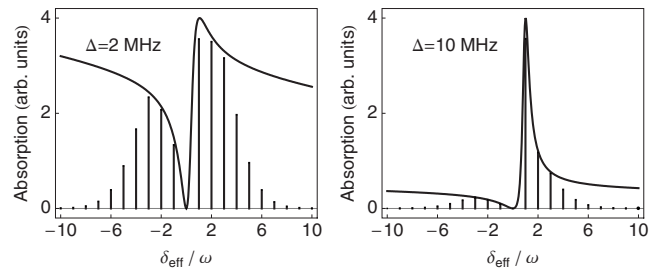


FIG. 3. The imbalance between sideband cooling ($\delta_{\text{eff}}/\omega > 0$) and sideband heating ($\delta_{\text{eff}}/\omega < 0$) is shown for two values of the detuning Δ . The full line gives the three-level EIT line shape. The bars indicate the strength of sideband transitions (summed over the lowest 100 vibrational levels of the HO) which are active when the two-photon detuning is set to $\delta=0$, the EIT minimum. ($\eta=0.25$, $\Gamma=2\pi \times 6$ MHz, $g_1=2\pi \times 1.4$ MHz, and $g_2=2\pi \times 0.1$ MHz).

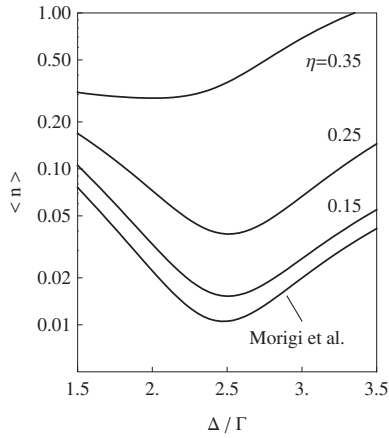


FIG. 4. Predictions for stationary vibrational population in EIT cooling limit at various values of η as a function of detuning Δ/Γ . Parameters are $\omega=\Gamma/10$, $g_1=\Gamma$, $g_2=\Gamma/10$.

standard three-level absorption line shape at the effective detuning $\delta_{\text{eff}}=\Delta n\omega$. This line shape is shown by the full curve in Fig. 3. The relative strength of individual sideband transitions is of course dictated by the Franck-Condon factors $|F(n, m, \eta)|$, the spread of significant sideband transitions being governed by the magnitude of η (compare with Fig. 2). The asymmetry in the absorption profile in the vicinity of the EIT minimum increases with increasing value of Δ and so does the imbalance between cooling transitions ($\Delta n < 0$) and heating transitions ($\Delta n > 0$). The imbalance is in favor of cooling when $\Delta > 0$. In Fig. 3 the Rabi frequency of the pump laser was chosen such that the absorption peak from the ac-Stark-shifted resonance falls on the first cooling sideband $\delta_{\text{eff}}/\omega = +1$. This is the optimal condition for EIT cooling in the Lamb-Dicke limit when only one sideband is active.

In the following we compare the predictions of our model with those in the Lamb-Dicke limit by examining the sensitivity of the mean vibrational level $\langle n \rangle$ in the stationary population to the parameters of pump detuning Δ , pump Rabi frequency g_1 , and trap-level frequency ω . The results in Figs. 4 and 5 show that the cooling degrades somewhat as the value of η increases. This is not unexpected as—in general—the preference for cooling transitions diminishes with increasing η at fixed values of the detuning Δ and the Rabi frequency g_1 . This is due to the fact that the width of the ac-Stark-shifted resonance mimics that of the EIT minimum and hence can cover only a limited number of sidebands for cooling.

On the other hand, the number of sidebands for heating transitions is practically unlimited as heating transitions may experience the entire natural width of the excitation profile, to the red of the EIT minimum. However, we see that even for relatively high values of η cooling is still efficient, albeit not to a nearly pure translational ground state, $\langle n \rangle \approx 0$. Also apparent from the right-hand side of Fig. 5 is the appearance of several additional minima as η is increased. These are due to the beneficial ac-Stark shifting of the absorption peak to the second and third higher sideband transitions when these gain strength at increasing values of η .

Figure 6 gives the dependence of cooling on the trap frequency ω in comparison to the Lamb-Dicke limit. Again the

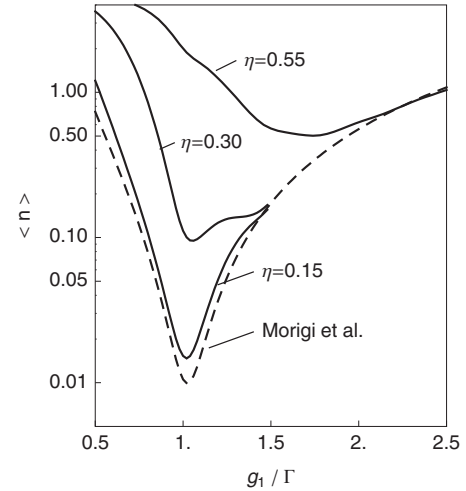


FIG. 5. Predictions for stationary vibrational population in EIT cooling limit at various values of η as a function of the Rabi frequency of the coupling laser g_1/Γ . Parameters are $\omega=\Gamma/10$, $\Delta=2.5\Gamma$, $g_2=\Gamma/10$.

appearance of additional minima points to the favorable ac-Stark shifting to higher sideband transitions. At a given value of g_1 (meaning a given separation between the EIT minimum and the ac-Stark-shifted resonance) this is accomplished at decreasing values of ω . All of these results underscore the importance of higher sidebands at even relatively low values of η . Note that the parameters used in the simulations in Figs. 4–6 are optimized for EIT cooling in the Lamb-Dicke limit rather than the specific parameter values of η used here, in order to facilitate comparison with the predictions in the Lamb-Dicke limit [14]. Beyond the Lamb-Dicke limit the separation between the EIT minimum and the ac-Stark-shifted resonance is more optimally chosen to be several times the trap energy—in order to cover several of the cooling sidebands—as will be shown below.

We now turn to the situation encountered for neutral Rb atoms in typical optical dipole traps, using the experimental parameters $\Gamma=2\pi \times 6$ MHz, $E_r=2\pi \times 3.6$ kHz. The trap parameters ω , η , and the Rabi frequencies are considered to be adjustable to the specific experimental situation. We first consider cooling rates. The time development of populations in the electronic state $|2\rangle$ is shown in Fig. 7. This state carries the dominant population when $g_1 \gg g_2$. The populations ρ_{11}

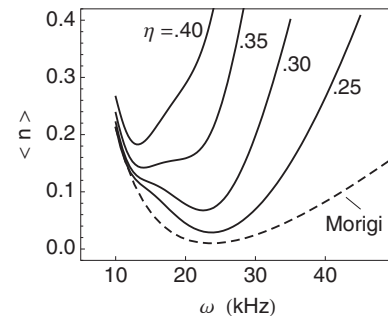


FIG. 6. Cooling limit as a function trap frequency, in comparison with the prediction in the Lamb-Dicke limit. Parameters are $\Delta=15$ MHz, $\Gamma=6$ MHz, $g_1=1.4$ MHz, $g_2=100$ kHz.

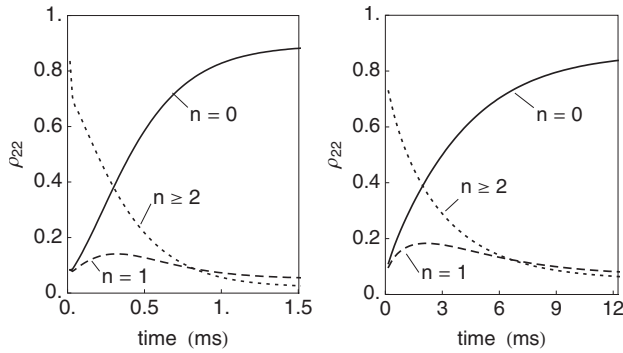


FIG. 7. Temporal development of cooling for $\eta=0.25$ (left-hand side) and $\eta=0.55$ (right-hand side). The full lines give the population in $n=0$, the dashed lines in $n=1$, while the dotted lines give the sum of populations in vibrational levels $n \geq 2$. Parameters are $\Delta = 20$ MHz, $\Gamma = 6$ MHz, $g_2 = 100$ kHz, and (left-hand side) $\omega = 58$ kHz, $g_1 = 3.2$ MHz, $\delta = 58$ kHz and (right-hand side) $\omega = 12$ kHz, $g_1 = 1.5$ MHz, $\delta = 6$ kHz.

are roughly g_1/g_2 times smaller than those of ρ_{22} , the populations ρ_{33} always stay at a level below 10^{-5} at the parameters used in Fig. 7. The initial conditions for the two simulations in Fig. 7 are that initially all ground-state levels are evenly populated. Regardless of the initial population distribution the simulations show that the same final stationary result is reached albeit at slightly different cooling time.

The cooling rates turn out to be comparable to those predicted in the Morigi *et al.* model [14]. Note that in the Lamb-Dicke limit the cooling rate increases as η increases since the strength of sideband transitions increase with the order $O(\eta^2)$. As η becomes too large, cooling is still active, however it reaches an equilibrium over an ever broader distribution of low vibrational levels as η increases. In choosing the laser parameters for the simulations in Fig. 7 we have roughly optimized the ratio of heating-to-cooling sidebands (see Fig. 3) by choosing the Rabi frequency g_1 in such a way that the ac-Stark-shifted resonance peaks at the second vibrational sideband for $\eta=0.25$ and at the third vibrational sideband for $\eta=0.55$. Also a slightly positive two-photon detuning δ has been assumed for reasons which become clear from the results shown in Fig. 8.

The results in Fig. 8 show the sensitivity of the stationary vibrational populations on the two-photon detuning δ . It is apparent that for efficient cooling, the two-photon detuning must be kept stable to a value better than the trap frequency ω in order to exploit the benefits of EIT cooling. These results also show that optimal cooling is achieved at small positive detunings δ unless η is very small ($\eta < 0.1$).

A primary conclusion from these results is that EIT cooling can indeed work at elevated values of the Lamb-Dicke parameter. Limitations appear when η reaches well above ≈ 0.5 when the width of heating sidebands overwhelms the necessarily restricted cooling wing of the EIT line shape. Some degree of selectivity in the effective value of η comes from the choice of angle between the two lasers and between the effective k vector $\delta\vec{k} = \vec{k}_1 - \vec{k}_2$.

For any experimental realization it is important to consider the dependence of the efficiency of the cooling process

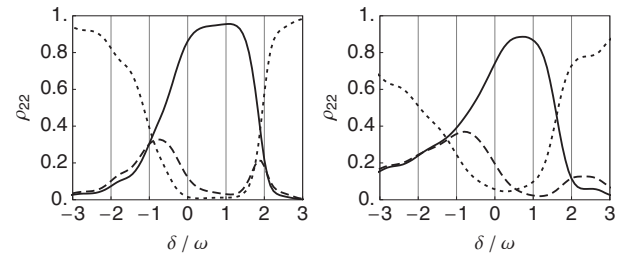


FIG. 8. The frequency sensitivity of the cooling window is apparent from this plot which gives the stationary population in the vibrational levels in the electronic state $|2\rangle$ as a function of the two-photon detuning δ . The plot on the left-hand side is for $\eta = 0.25$, the plot on the right-hand side is for $\eta = 0.55$. The full lines give the population in $n=0$, the dashed lines in $n=1$, while the dotted lines give the sum of populations in vibrational levels $n \geq 2$. Parameters are the same as those in Fig. 7.

on the laser frequency stability. We have so far silently considered the case of perfectly stabilized lasers. For nearly all EIT effects the magnitude of the stability of the difference frequency of the two lasers matters, rather than the stability of each individual laser [22]. In EIT cooling the effects of laser stability are twofold, for one the window of efficiency for cooling is of the order of or smaller than the vibrational trap frequency (see Fig. 8) and second the suppression of carrier transitions relative to the absorption at the ac-Stark-shifted resonance diminishes proportional to the magnitude of δ/ω . Hence, the prerequisite for EIT cooling is a stability and controllability of the laser-frequency difference to a precision better than the trap frequency. Similar demands hold for the ground-state energy difference ω_{12} , thus placing stringent requirements on an EIT cooling experiment when trap frequencies are low.

In real world applications to clouds of trapped atoms, phase-changing collisions will place a lower limit on the dark-state lifetime and hence the EIT width. This restricts atom densities that one can achieve with EIT cooling, as the dark state lifetime must exceed the vibrational time scale, $2\pi/\omega$, in order for EIT cooling to become effective. Reabsorption of spontaneous photons from the very weakly populated excited level will pose an additional cooling limit for a dense atom cloud.

The model simulations presented here assume identical vibrational frequencies in the three electronic states. This is an excellent assumption for trapped ions as the trap depth is only very weakly modified by the electronic-state-dependent Stark effect. The situation is different for neutral atoms in optical dipole traps for which the state-dependent polarizability dictates the trap depth. As a result the trap frequencies will in general be different for each of the three electronic states involved in an EIT scheme, unless a situation of a magic wavelength [23] for the dipole-trap laser can be found. If not it appears best to choose a trap-laser wavelength well red of the lowest energy excited state transition. In this far-red-detuning regime the polarizabilities are not greatly different [24,25] and the excited electronic state is indeed bound in the dipole trap. In this case and when the trapping frequencies are much smaller than the detuning Δ , the requirement of blue detuning can be met for even high side-

band transitions and the requirements for EIT cooling can be fulfilled.

IV. CONCLUSIONS

We have studied a three-level atom trapped in a one-dimensional harmonic oscillator, interacting with two laser beams. Preparing the condition of electromagnetically induced transparency leads to a cancellation of the carrier transitions (vibrationally diagonal transitions) which are a source of heating when spontaneous emission is involved. In addition, when choosing blue detuning of the pump laser and a suitable ac-Stark shift induced by this laser, two-photon sideband transitions which cool can occur at a higher rate than those which heat. We show here that this miracle of cooling via EIT can be realized even in the case that higher-order sidebands are active. Our approach allows for the optimization of cooling in realistic trap environments.

APPENDIX A: ANGULAR DISTRIBUTION IN SPONTANEOUS EMISSION

In the spontaneous emission process, the atomic center-of-mass can gain a recoil from the spontaneously emitted photon. Such a momentum change is described by the momentum shift operator $\exp[-i\vec{k}\cdot\vec{r}]$, which acts on the atomic center-of-mass state vector as [20]

$$e^{-i\vec{k}\cdot\vec{r}}|\vec{p}\rangle = |\vec{p} - \hbar\vec{k}\rangle, \quad (\text{A1})$$

where $|\vec{p}\rangle$ is a momentum eigenstate.

The wave vector of the emitted photon can be written as $\vec{k} = k\hat{n}$, where \hat{n} is the direction of the spontaneously emitted photon. With (A1) we can relate initial and final states

$$|\Psi\rangle_f = e^{-i\vec{k}\cdot\vec{r}}|\Psi\rangle_i = e^{-ik\hat{n}\cdot\vec{r}}|\Psi\rangle_i, \quad (\text{A2})$$

and as density matrix element

$$\hat{\rho} = |\Psi\rangle_{ff}\langle\Psi| = e^{-ik\hat{n}\cdot\vec{r}}|\Psi\rangle_{ii}\langle\Psi|e^{ik\hat{n}\cdot\vec{r}}. \quad (\text{A3})$$

Denoting the spatial distribution of the spontaneous photons as $\Xi(\hat{n})$, the probability of scattering photons into the solid angle $d\Omega$ with the rate of Γ is $\Gamma\Xi(\hat{n})d\Omega$. The rate of populating the ground state in spontaneous emission is then

$$\Gamma\Xi(\hat{n})d\Omega e^{-ik\hat{n}\cdot\vec{r}}|\Psi\rangle_{ii}\langle\Psi|e^{ik\hat{n}\cdot\vec{r}}, \quad (\text{A4})$$

where $|\Psi\rangle_i = |e\rangle \otimes |n\rangle_i$, the initial atomic center-of-mass state being $|n\rangle_i$. In this way the probability of populating a ground-state vibrational level $|n\rangle_j$ is

$$\begin{aligned} & \Gamma\Xi(\hat{n})e^{-ik\hat{n}\cdot\vec{r}}|3\rangle \otimes |n\rangle_{ii}\langle n| \otimes \langle 3|e^{ik\hat{n}\cdot\vec{r}}d\Omega \\ & = \Gamma\Xi(\hat{n})\rho_{33}e^{-ik\hat{n}\cdot\vec{r}}\hat{\sigma}e^{ik\hat{n}\cdot\vec{r}}d\Omega. \end{aligned} \quad (\text{A5})$$

This term needs to be integrated over the angular distribution of spontaneous photons. If Γ_j is the rate of spontaneous emission into the ground-state level j we obtain for its probability

$$\tilde{\rho}_{jn,jn} = \Gamma_j \int \Xi(\hat{n})|j\rangle\langle 3|e^{-ik\hat{n}\cdot\vec{r}}\hat{\sigma}e^{ik\hat{n}\cdot\vec{r}}|j\rangle\langle 3|d\Omega. \quad (\text{A6})$$

Assuming that spontaneous emission is always along the HO axis, we can omit integration and obtain for the second term on the right-hand side of Eq. (15),

$$\sum_{j=1}^2 \Gamma_j |j\rangle\langle 3| (e^{iq_j x} \hat{\rho} e^{-iq_j x}) |3\rangle\langle j|. \quad (\text{A7})$$

APPENDIX B: TRANSITION MATRIX ELEMENTS

In Eq. (12) we have used the momentum shift operator $\exp[\pm i\vec{k}\cdot\vec{x}]$, where \vec{k} is the laser beam wave vector and \vec{x} is the position of atomic center-of-mass in Cartesian coordinates. The term $\vec{k}\cdot\vec{x}$ can be rewritten, using the inner product, as

$$\vec{k}\cdot\hat{x} = |k||x|\cos(\vec{k}\cdot\hat{x}) = |k||x|\cos(\theta). \quad (\text{B1})$$

The center-of-mass position in the quantum mechanical harmonic oscillator is defined in terms of annihilation and creation operators,

$$\hat{x} = \sqrt{\frac{\hbar}{2M\omega}}(\hat{a} + \hat{a}^\dagger). \quad (\text{B2})$$

Introducing the Lamb-Dicke parameter

$$\eta = |k| \sqrt{\frac{\hbar}{2M\omega}} \cos(\theta), \quad (\text{B3})$$

and applying the Baker-Campbell-Hausdorff relation [16] we may write

$$e^{\pm i\eta(\hat{a} + \hat{a}^\dagger)} = e^{-\eta^2/2} \sum_{l=0}^{\infty} \frac{(i\eta\hat{a}^\dagger)^l}{l!} \sum_{l'=0}^{\infty} \frac{(i\eta\hat{a})^{l'}}{l'!}. \quad (\text{B4})$$

Taking into account the relations

$$(\hat{a}^\dagger)^l |n\rangle = \sqrt{\frac{(n+l)!}{n!}} |n+l\rangle, \quad (\text{B5})$$

$$(\hat{a})^{l'} |n\rangle = \sqrt{\frac{n!}{(n-l')!}} |n-l'\rangle, \quad (\text{B6})$$

and using the expansion (B4) our Franck-Condon factor (12) can be written as

$$F(n, m, \eta) = e^{-\eta^2/2} \sum_{l=0}^{\infty} \sum_{l'=0}^{\infty} \frac{(i\eta)^{l+l'} \sqrt{m! (m-l'+l)!}}{l! l'! (m-l')!} \delta_{n, m-l'+l}. \tag{B7}$$

The products from the double sum are zero except when $l = n - m + l'$. Hence, the possible l' values range from $l'=0$ to $l'=m$ when $n \geq m$, while the range is from $l'=m-n$ to l'

$=m$ when $n \leq m$. This leaves us with the single sum

$$F(n, m, \eta) = e^{-\eta^2/2} \sum_{l'=l'_{\min}}^m \frac{(i\eta)^{2l'+n-m} \sqrt{m! n!}}{l'! (l'+n-m)! (m-l')!}, \tag{B8}$$

with $l'_{\min} = \text{Max}[0, m-n]$.

[1] M. H. Anderson *et al.*, *Science* **269**, 198 (1995).
 [2] K. B. Davis *et al.*, *Phys. Rev. Lett.* **75**, 3969 (1995).
 [3] M. Lewenstein and L. You, *Adv. At. Mol. Phys.* **36**, 221 (1996).
 [4] J. Javanainen and S. Stenholm, *Appl. Phys.* **24**, 151 (1981).
 [5] W. Neuhauser, M. Hohenstatt, P. Toschek, and H. Dehmelt, *Phys. Rev. Lett.* **41**, 233 (1978); D. J. Wineland, R. E. Drullinger, and F. L. Walls, *ibid.* **40**, 1639 (1978).
 [6] A. Aspect, E. Arimondo, R. Kaiser, N. Vansteenkiste, and C. Cohen-Tannoudji, *Phys. Rev. Lett.* **61**, 826 (1988).
 [7] F. Schmidt-Kaler *et al.*, *Appl. Phys. B: Lasers Opt.* **73**, 807 (2001).
 [8] M. Kasevich and S. Chu, *Phys. Rev. Lett.* **69**, 1741 (1992).
 [9] F. Diedrich, J. C. Bergquist, W. M. Itano, and D. J. Wineland, *Phys. Rev. Lett.* **62**, 403 (1989).
 [10] J. Javanainen and M. Lindenberg, *J. Opt. Soc. Am. B* **3**, 1008 (1986).
 [11] C. Cohen-Tannoudji, J. Dupont-Roc, and G. Grynberg, *Atom-Photon Interactions* (Wiley, New York, 1992).
 [12] I. Marzoli *et al.*, *Phys. Rev. A* **49**, 2771 (1994).
 [13] G. Morigi, J. I. Cirac, M. Lewenstein, and P. Zoller, *Europhys. Lett.* **39**, 13 (1997).
 [14] G. Morigi, J. Eschner, and C. H. Keitel, *Phys. Rev. Lett.* **85**, 4458 (2000).
 [15] G. Morigi, *Phys. Rev. A* **67**, 033402 (2003).
 [16] M. Orszag, *Quantum Optics* (Springer, Berlin, 2000), pp. 276–281.
 [17] B. Karl, *Density Matrix Theory and Applications* (Plenum, New York, 1981).
 [18] L. You, M. Lewenstein, and J. Cooper, *Phys. Rev. A* **51**, 4712 (1995).
 [19] This is the origin for Doppler-free EIT line shapes in thermal atoms, see, for example, [22].
 [20] P. Meystre, *Atom Optics* (Springer, New York, 2001).
 [21] Typically $m_m=10$ for $\eta=0.1$, increasing to $m_m=25$ for $\eta=0.5$.
 [22] M. Erhard and H. Helm, *Phys. Rev. A* **63**, 043813 (2001).
 [23] J. McKeever, J. R. Buck, A. D. Boozer, A. Kuzmich, H. C. Nagerl, D. M. Stamper-Kurn, and H. J. Kimble, *Phys. Rev. Lett.* **90**, 133602 (2003).
 [24] C. Krenn *et al.*, *Z. Phys. D* **41**, 229 (1997).
 [25] For rubidium the dc polarizabilities of ground and excited states differ by about a factor of 2.7 [24].